ELSEVIER

Journal of Nuclear Materials 264 (1999) 198–205

journal of nuclear materials

A many body potential for α-Zr. Application to defect properties

R.C. Pasianot [a,b,*], A.M. Monti [a]

[a] *Dpto. de Materiales, Comisión Nacional de Energía Atómica, Av. Rivadavia 1917, 1033, 1429 Buenos Aires, Argentina*
[b] *CONICET, Av. Rivadavia 1917, 1033, Buenos Aires, Argentina*

Received 26 December 1997; accepted 12 June 1998

Abstract

An embedded atom model (EAM) interatomic potential that reproduces room temperature elastic behavior for α-Zr is developed. At variance with previous potentials from the literature, the present one predicts a self-interstitial relaxation volume consistent with the relatively low measured value. A critical review of results for static and dynamic properties of point defects is undertaken by comparing with predictions from other potentials and with experimental findings. This survey allows us to conclude that most well fitted EAM potentials give low vacancy migration energies and a basal crowdion as the stable interstitial configuration with fast 1D migration.

PACS: 61.72.-y; 61.72.Ji; 66.30.Fq

1. Introduction

There have been several attempts in the literature to develop simple many-body interatomic potentials for the hcp structure. These potentials aim to reproduce as closely as possible the experimental values of the five elastic constants and the *c/a* ratio, these being relevant properties for the determination of the long range displacement field and defect anisotropy, respectively. Oh and Johnson [1,2] used Voigt averages for bulk and shear moduli to approximately match the elastic constants, with almost ideal *c/a* ratio in [1] for Mg, Zr and Ti and a more realistic value in [2] for Zr. Igarashi et al. [3] were the first to develop EAM type potentials [4,5] for a number of hcp metals (Zn, Mg, Co, Zr, Ru, Ti, Hf and Be) attempting to exactly match those properties; however the inner strain contribution to the elastic constants was neglected. Accounting for this term, Pasianot and Savino [6] found that EAM type potentials impose restrictions on the elastic constants of an hcp structure, among them,

$$(3C_{12} - C_{11})/2 > C_{13} - C_{44}, \tag{1}$$

and reported potentials for some hcp metals (Co, Mg, Ti, Hf) exactly matching the experimental values of the five elastic constants and the *c/a* ratio. It is worth noting that the above condition is strongly violated for Zn and Cd and only slightly for Zr at 0 K. Using an approximate parametrization scheme for Ti and Zr, Ackland [7,8] developed EAM type potentials that fit the *c/a* ratio within a fraction of 1% and reasonably well the low temperature experimental elastic constants [9], with departures of about 10% for C_{33} and C_{13} in Ti and 25% for C_{12} in Zr. Also for Zr, Goldstein and Jónsson [10] reported an EAM that accounts for inner strains, though due to their fitting scheme all the elastic constants are matched within 5% except C_{44} which is larger by 25%, being the *c/a* ratio well reproduced.

The aim of the present study is to develop an EAM potential for Zr to be used in the computer simulation of defects, as well as to carry out a consistent comparison with predictions of other selected potentials and with experimental findings in an effort to assess the reliability of the model.

The work is organised as follows: Section 2 is devoted to the potential; results for point defects and small

* Corresponding author. E-mail: pasianot@cnea.edu.ar.

0022-3115/99/$ – see front matter
PII: S0022-3115(98)00477-2

vacancy clusters are reported in Section 3; in Section 4 the results are discussed, and finally Section 5 gives a brief summary and advances some perspectives for future work.

2. The interatomic potential. General considerations and construction

In EAM type approaches [4,5], the energy of an atomic assembly is written as a summation over sites, each term being

$$E_i = \sum_j V(R_{ij}) + F(\rho_i), \tag{2}$$

where V stands for a pair potential, F is the so called embedding function and ρ is interpreted as a local electronic density built by a superposition of pair-like functions

$$\rho_i = \sum_j \varphi(R_{ij}). \tag{3}$$

It has been pointed out by several authors [11–14] that the isotropic interaction embodied in the many-body term of Eq. (2) is not able to represent covalent aspects possibly important in transition metals. Evidence for this is given for instance by the negative values of the Cauchy pressure of Cr (bcc), and Be and Y (hcp), C_{12}–C_{44} and C_{13}–C_{44}, respectively. Further developments of the EAM form including angular terms are able to alleviate this pitfall [11,14]; however, the constraint imposed by Eq. (1) seems to be of a different nature. In this sense it is interesting to write it down for a cubic fcc crystal in which axis [1 1 1] is brought into coincidence with axis [0 0 0 1] of the hcp lattice, such that the stacking sequence ABAB... is turned into ABCAB... Directions 1, 2 and 3 stand now for $[1\,\bar{1}\,0]$, $[1\,1\,\bar{2}]$ and [1 1 1], respectively. Denoting by E_{ij} the elastic constants in this frame and by C_{ij} those in the standard cubic one, the result obtained is

$$\frac{3E_{12} - E_{11}}{2} > E_{13} - E_{44} \Longleftrightarrow (C_{11} - C_{12}) + C_{44} > 0, \tag{4}$$

where the right-hand side must be true for any elastically stable cubic lattice.

Considering that Eq. (1) is satisfied for Zr at room temperature, an interatomic potential of the EAM type is developed. The fitting procedure, next outlined, follows Ref. [6]. Without loss of generality $F(\rho)$ is imposed to have null first derivative at the perfect lattice density ρ_0, this makes V(R) an 'effective pair potential'. The atomic electronic function φ is chosen as a Thomas–Fermi like screening function continuous up to the second derivative and smoothly matched to zero at the cut-off distance R_c,

$$\varphi(x) = \varphi_0 f(x), \tag{5}$$

$$f(x) = \begin{cases} \exp(-5x)/x, & x \leqslant R_m, \\ (x - R_c)^3(a_1x^2 + a_2x + a_3), & R_m < x \leqslant R_c, \\ 0, & R_c \leqslant x, \end{cases}$$

where φ_0 is a constant selected such as $\rho_0 = 1$, x is measured in basal lattice constant units and the other parameters are reported in Table 1. $V(x)$ is given the form of a seven-piece cubic polynomial continuous up to the second derivative according to

$$V(x) = \sum_{k=1}^{7} A_k (x_k - x)^3 H(x_k - x) \tag{6}$$

$H(x)$ being the Heaviside step function, x_k knot points (adequately chosen) and A_k coefficients determined through the fitting procedure; both sets of values are quoted in Table 1. Notice the above equation permits some control of the repulsive wall by including knots for distances below first neighbours, without spoiling the fitting to perfect lattice properties. These seven coefficients plus F_0 and F_0'', embedding function and its second derivative at the perfect lattice, constitute nine unknowns exactly solved for through a system of equations [6] involving the two lattice parameters a and c, the cohesive energy E_C, the five elastic constants and an

Table 1
Potential parameters, $V(x)$ is in eV, x_k in units of the basal lattice parameter and φ is dimensionless

	k	x_k	A_k			
	1	1	−38.4084159			
	2	1.05	36.9240324			
$V(x)$	3	1.55	−6.0670690			
	4	1.60	8.4563250			
	5	1.65	−4.6893208			
	6	1.70	7.9557179			
	7	1.75	−5.6449389			
	a_1	a_2	a_3	R_m	R_c	φ_0
$\varphi(x)$	−0.44417136	1.07926027	−0.67936231	1.3	1.65	11.28516908

Table 2
Experimental values exactly fitted, a in nm [15], E_c [16] and E_v^f [17] in eV and C_{ij} in eV/nm^3 [9]. In parentheses percental deviation from 4 K data

a	c/a	E_c	E_v^f	C_{11}	C_{12}	C_{13}	C_{33}	C_{44}
0.3232	1.593	6.25	1.74	895.1	454.4	407.6	1028.1	199.7
				(8.4)	(−7.7)	(−1.1)	(4.7)	(13.4)

approximate value for the vacancy formation energy E_v^f. These quantities are all reported in Table 2, together with the percental deviation of the elastic constants at room temperature, exactly fitted by the potential, with respect to 4 K data. Notice the maximum deviation is somewhat lower than the ones quoted in the previous section for other potentials.

In order to extend the domain of F(ρ) to densities beyond the vicinity of the perfect lattice value, Eq. (2) is constrained to satisfy Rose's et al. universal equation of state [18]. This is also a way of partly providing information on interactions for shorter than first neighbours distances. Such an equation gives the energy of uniformly compressed or dilated lattices through a scaled variable,

$$E(\tilde{a}) = -E_C(1+\tilde{a})\exp(-\tilde{a}) \tag{7}$$

with

$$\tilde{a} = 3[\Omega B/E_C]^{1/2}(a/a_0 - 1),$$

where Ω is the atomic volume, B the Voigt average bulk modulus and a_0 the basal lattice parameter at equilibrium (zero stresses). $F(\rho)$ is numerically obtained by equating the left-hand side of Eq. (2) to Eq. (7) and subtracting the pair term of Eq. (6), ρ being computed simultaneously according to Eq. (3). The potential is depicted in Fig. 1.

We note that the potential third derivative is discontinuous at the knot points, some of which resulted very close to lattice nodes. Besides, the second derivative shows an oscillatory behavior at the very potential tail, where there are two shells of 18 neighbours. The so deduced potential predicts a stable hcp structure ($E_C = 6.25$ eV) with respect to other common crystal structures such as fcc ($E_C = 6.23$ eV) and bcc ($E_C = 6.20$ eV) and a positive I_2 stacking fault energy ($\gamma = 69.4$ mJ/m^2), the latter being essentially controlled by varying the cut-off radius.

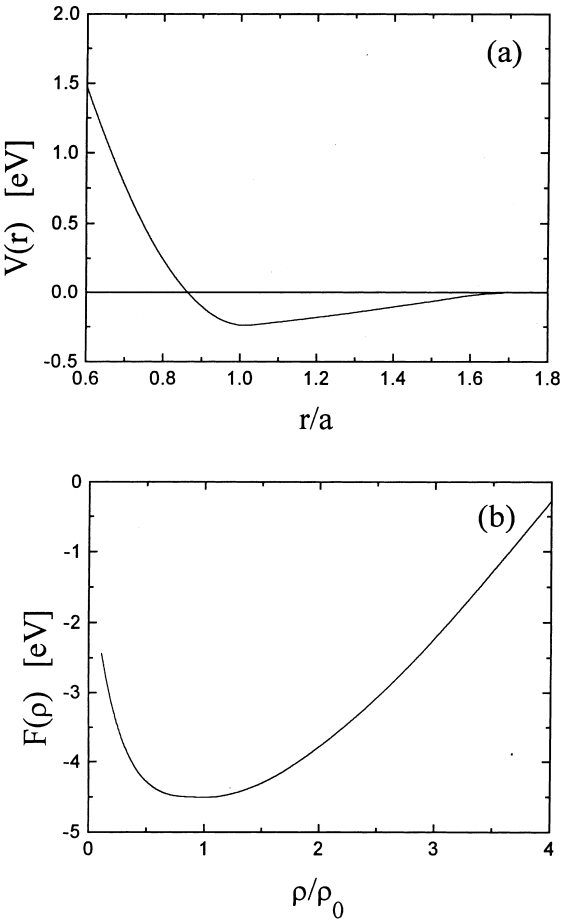

Fig. 1. Interatomic potential for Zr: (a) effective pair interaction; (b) embedding function.

3. Results

The calculations performed refer to point defects and small vacancy clusters. Defect structure computations are carried out with static relaxation based on the conjugate gradients technique [19], which allows us to compute formation and migration energies, as well as dipole tensors and relaxation volumes [20,21]. Atomic eigenfrequencies are obtained by either diagonalizing the force constant matrix for each individual atom or for a cluster of atoms surrounding the defect [20]. Frequencies are used for entropy calculations and to determine the stability of a given configuration, this including the search of migration saddle points. Molecular dynamics [22] are also used to study the thermal perfect lattice behavior. Related to this, it must be pointed out that the potential, though appropriate for the calculation of lattice frequencies, which depend on first and second

Table 3
Computed magnitudes for vacancy formation and migration: energies E (eV), entropies S (Boltzmann's constant, k_B) and relaxation volumes V^r (at.vol.). Columns labelled Vac, A-jump and B-jump refer to the relaxed vacancy, non-basal and basal jumps, respectively

	Vac	A-jump	B-jump
E	1.74	0.59	0.57
S	4.15	6.36	5.93
V^r	−0.20	−0.25	−0.29

derivatives, is not for their variations as the lattice is expanded or contracted, which depend on the third one. Consequently, the lattice thermal expansion is badly predicted, contracting on the basal plane up to about 200 K and expanding afterwards, while the c-axis always expands.

Table 3 reports the computed values for the vacancy formation and migration energies E_v^f and E_v^m, as well as entropies S_v^f and S_v^m, and the corresponding relaxation volumes V^r; entropy refers to independent oscillators for constant pressure condition.

The studied clusters of n vacancies, schematically depicted in Fig. 2, are those of highest binding free energy G^b found in [23] and such that this quantity increases with n. The results quoted in Table 4 are: binding energy E^b defined as $E^b = (nE_v^f - E_{nv}^f)/n$ where E_{nv}^f is the formation energy for a given cluster, relaxation volume V^r, formation entropy S^f and binding free energy G^b defined as for E^b. Positive values for binding energies indicate tendency to clustering.

Table 4
Computed magnitudes for vacancy clusters: binding energy E^b (eV), relaxation volume V^r (at.vol.), formation entropy S^f (k_B), and binding free energy at 1000 K G^b (eV)

	E^b	V^r	S^f	G^b
2.1	0.11	−0.40	8.01	0.09
2.2	0.12	−0.41	7.57	0.08
3.1	0.23	−0.73	11.35	0.20
3.2	0.23	−0.49	8.86	0.12
3.3	0.22	−0.65	11.71	0.20
4.1	0.33	−0.51	10.39	0.19
5.1	0.40	−0.43	10.77	0.22
7.5	0.39	−1.50	21.62	0.30

Finally in Table 5 we report formation energies and relaxation volumes for standard selfinterstitials configurations (see e.g. Fig. 2 in Ref. [21] for details): basal crowdion B_C, basal dumbbell B_S, basal octahedral B_O, crowdion C, basal tetrahedral B_T, octahedral O, tetrahedral T and axial dumbbell S. A unique feature of our potential is that the calculated interstitial relaxation volume is in reasonable agreement with the relatively low experimental value of $V_i^r = 0.6 \pm 0.15\Omega$ [24]. Vibration mode analysis shows that all the configurations, except B_C and B_S, do possess imaginary eigenfrequencies,

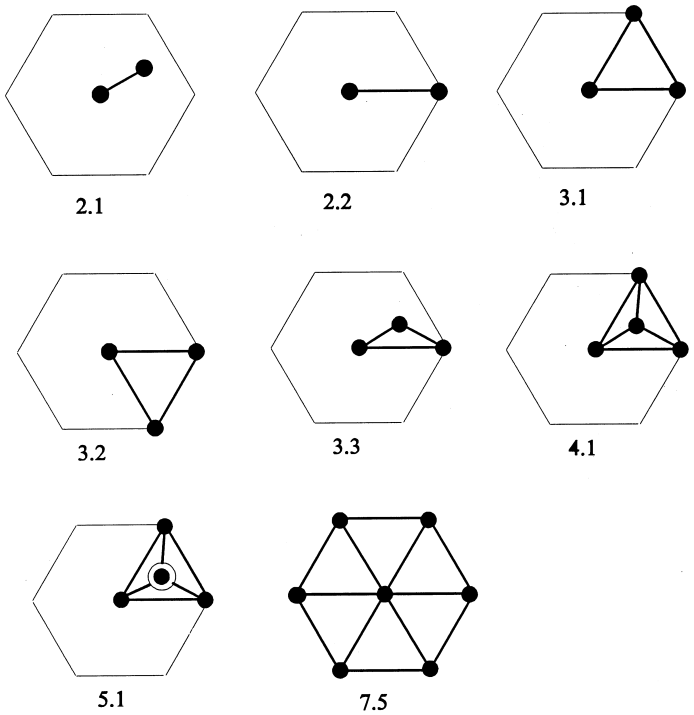

Fig. 2. Scheme and naming convention for the considered vacancy clusters.

Table 5
Self-interstitial formation energies (eV) relative to the stable configuration E^f (B_c) = 2.50 eV and relaxation volumes (at.vol.)

	B_c	B_s	B_o	C	B_T	O	T	S
E^f	0.00	0.01	0.13	0.28	0.30	0.30	Unst.	0.54
V^r	0.86	0.87	0.77	0.91	0.92	1.06		0.70

meaning instability. For B_C, real eigenfrequencies are obtained by using a coupled cluster of about 150 atoms comprising the defect; the same holds for B_S though one eigenfrequency results very low. In this mode both atoms of the dumbbell vibrate with high amplitude along the close-packed direction coincident with the defect axis. This fact plus the low energy difference between the configurations of about 0.01 eV suggests a high unidirectional mobility. The possibility of B_C reorientation to escape from its atom row is also explored, finding a migration energy of 0.13 eV for jump BB′ depicted in Fig. 3; notice this is geometrically different from jump BB″, for which no saddle point was found.

4. Discussion

Present results are compared with those obtained from other potentials [2,7,8,10,21] either computed by us when necessary, or taken from the literature.

Table 3 shows vacancy migration energies of about $E_v^m = 0.56$ eV, slightly favouring jumps on the basal plane. Similar values and jump anisotropy are predicted by other realistic EAM potentials modeling Zr: 0.86 [8], 0.63 [10] and 0.78 [2], the first two calculated by us and the latter reported in the original reference. It should be noted that, within the framework of semiempirical interaction models, E_v^m and V_i^r are strongly correlated magnitudes both depending on the potential stiffness at similar interaction distances; in this sense the above E_v^m values from [8,10,2] may be in excess because, contrary to ours, their predicted V_i^r overestimate the experimental value [24] by about 50%. The above vacancy migration energies are at variance with higher previous estimates from non-equilibrium short range pair potentials fitted to ideal *c/a* ratio e.g. 1.15 eV [25] and 1.47 eV [26], which in addition give the opposite anisotropy. The present results are however consistent with experimental findings based on positron annihilation (PAS) techniques that estimate a value in the range 0.6–0.7 eV [27]. Such an unexpectedly low value was later ascribed to an effect produced by trace levels of the ultra-fast diffuser Fe, migrating through Fe-vacancy pairs [28]. Although the enhancement of selfdiffusion due to Fe impurities has been established beyond doubt [29], PAS experiments using high purity Zr samples [30] have not been conclusive in either accepting or rejecting the low value of E_v^m as being due to Fe impurities. Low values of E_v^m do have important implications on E_v^f when considering recent selfdiffusion experiments on high purity Zr single crystals [31], for which an activation energy $Q = 3.17$ eV was obtained, somewhat lower than previous meausurements extrapolated for low temperatures [32]. By assuming a standard vacancy mechanism $Q = E_v^f + E_v^m$, the above value gives $E_v^f \approx 2.5$ eV. This is higher than the semiempirical expectation of about 1.8 eV [17] but not inconsistent with experimental results from PAS [17, 30] that stated the lower bound of 1.5 eV.

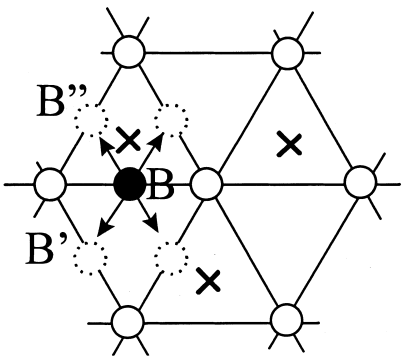

Fig. 3. Possible migration paths for the basal crowdion interstitial, B_C, leading to reorientation.

Going back to Table 3, it is seen that migration energies favor diffusion on the basal plane while migration entropies favor the opposite; a similar behavior is found for the other EAM potentials. It should be pointed out that reliable entropy values are very difficult to obtain because they depend on fine potential details not normally controlled in the fitting procedure. This is illustrated by the quite different predictions of the preexponential factor for self-diffusion D_0: 2×10^{-2}, 3.4×10^4 and 3×10^{-6} m^2/s, calculated for the present potential and for the ones of Refs. [8,2] respectively, the experimental result [31] being $D_0 = 9.0 \times 10^{-5}$ m^2/s.

Making reference to the small vacancy clusters considered, Table 4 shows higher relaxation volumes for clusters on the basal plane with both, top and bottom sides, bounded by atoms (cases 3.1 and 7.5); this is a signal of vacancy loop nucleation. Previous calculations [20] carried out with short range EAM-type potentials fitted to Voigt averages for the elastic constants, predict lower values than the present ones, the discrepancy being larger for clusters on the basal plane. Also shown in Table 4 is the increase of binding energy with cluster

size; this is in agreement with calculations from [20,24,33], the latter using a pair potential built in terms of local pseudopotential theory. Present results are however up to twice those of [33] for basal clusters and up to five times for void-type clusters (4.1 and 5.1). The reported positive formation entropies are in line with the general lattice softening, and higher for clusters with larger relaxations. Taking E^b as a measure of stability, our results would indicate that 3D clusters (e.g. 5.1) could be as stable as 2D ones on the basal plane; however by considering the vibrational entropy contribution to the binding free energy G^b, last column in Table 4, the latter clusters are favored. This is the same conclusion reached in [33], though those authors base their statement on configurational energy analysis only.

Regarding the self-interstitials, Table 5 suggests configurations can be grouped according to their formation energy in three sets: (i) B_C and B_S, the first being marginally stable with respect to the second, (ii) B_0, C, B_T, O, (iii) S and T. The same classification is obtained for other potentials including Ti [2,7,8,10,21] though details vary. Actually Ref. [10] seems to have not considered B_S; also neither B_C nor B_S were considered in Ref. [2]; simulations by the present authors using the potential ZRA of [2] give B_S as the stable interstitial, contrary to the reported one B_O , whereas for their ZRB (fitted to ideal *c*/*a* ratio) about the same energy is predicted for (the reported) C and (the here calculated) B_S . The evidence is therefore that these two configurations, B_C and B_S, are always predicted as the minimum energy ones by realistic EAM-like potentials for Zr and Ti.

From the experimental side there are apparently conflicting results. In one experiment, Exp. I from now on, X-ray Huang diffuse scattering (HDS) was performed on electron irradiated single crystals at liquid helium temperatures [24]; interstitial configurations consistent with O, S or T (all tetragonal in symmetry) were reported as possible candidates. The only other configuration considered, B_C (orthorhombic), was discarded on the grounds that the measured ratio for the axial/basal dipole components, 1.1 ± 0.2., was much higher than expected. The authors advocated the view of a high percentage of correlated recovery that could be the outcome of an interstitial–vacancy distance particularly small or a preferentially 1 or 2D interstitial migration.

In another experiment, Exp. II from now on, the internal friction technique was employed on neutron irradiated polycrystalline wires at 77 K [34]; 'frozen free split' peaks [35] with reorientation energies $E_R^1 = 0.17$ eV and $E_R^2 = 0.27$ eV, respectively, located at 72 and 115 K were proposed. The authors concluded that their results were best explained assuming a monoclinic defect undergoing 3D migration.

Unfortunately, in Exp. I no HDS measurements were undertaken that could reveal coupling between axial and basal components of the dipole tensor, namely invariant $\pi^{(2)} = P_{13}^2 + P_{23}^2$ [36]; this is null for all the configurations here considered but C. We also note that components P_{13} and P_{23} have no bearing on the (reported) interstitial relaxation volume. With respect to Exp. II, according to general anelasticity criteria [35] applied to the hcp structure only monoclinic or triclinic defects may give rise to internal friction split peaks. This leaves us just with configuration C among the common ones, which belongs to the former class. We recall split peaks may appear if there is one defect elementary jump much faster than any other that contributes to some but not all of the compliances undergoing relaxation. Such a situation may arise for compliance S_{44} among the two relevant to this configuration (S_{44} and S_{11}–S_{12}). This implies C would fit in this picture provided there exists a jump that is orders of magnitude faster than any other, contributing only to S_{44} relaxation. Fig. 4 explains the point; C interstitials are grouped in two sets, C^+ and C^-, according to their axial coordinate $\pm c/4$ respectively, each set having three possible orientations A, A′, A″. Therefore, transitions C_A^+–C_A^+ do not produce relaxation, those of C_A^+–$C_{A'}^+$ or C_A^+–$C_{A''}^+$ affect S_{11}–S_{12}, those of C_A^+–$C_{A'}^-$ or C_A^+–$C_{A''}^-$ relax both compliances, finally those of C_A^+–C_A^- relax only S_{44} and are the ones that would have to be the fastest.

The above might be supported by present calculations, in spite that C configuration is not predicted the minimum energy one. It was previously mentioned that C interstitial is found unstable for our potential; the same happens for potential of Ref. [2] though those of Refs. [10,8] produce a metastable configuration. When mode analysis is performed on the latter, real vibration eigenfrequencies are obtained, a few of them being very small. Particularly, in the smallest frequency mode the interstitial vibrates along the line AA of Fig. 4 concentrating about 50% of the kinetic energy. Such a mode, eventually combined with others of low frequency, could carry the interstitial through either site O or B_O. The first path, relatively high in energy (0.14 eV) and thus slow, would contribute mainly to transitions C^+–C^+; the second path, implying no energy expense (some −0.01 eV) and thus fast, would contribute mainly to transition C_A^+–C_A^-. Summarising, this argument gives the C configuration some chance to be consistent with the experimental findings of Ref. [34].

5. Summary

An EAM type potential for Zr fitted to room temperature elastic constants [9] and that accounts for the experimental self-interstitial relaxation volume has been developed. The potential, as well as other EAMs, is consistent with the low measured E_v^m [27]. New PAS experiments on high purity Zr single crystals [30] were

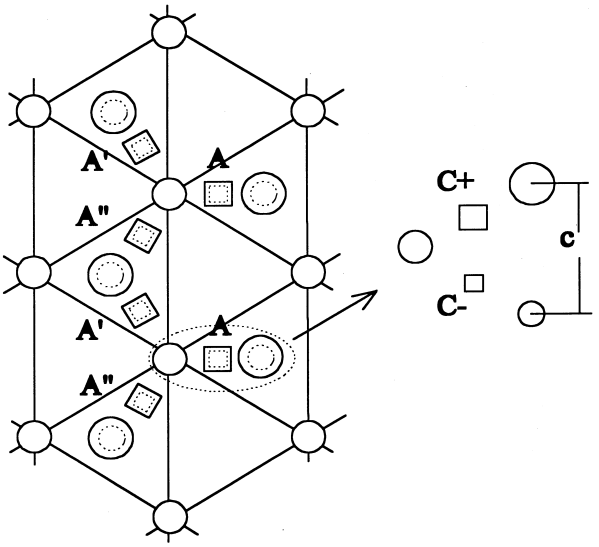

Fig. 4. The two families of crowdion interstitials, C^+ and C^-, as seen by anelastic relaxation. Symbol sizes refer to c-axis coordinate.

unable to either confirm or disprove the previous finding. This, when considering the relatively high selfdiffusion Q value measured recently [31], casts some doubt on the accepted E_v^f (fitted by the potential) that should probably be larger. In such a case no particular difficulty is anticipated for the potential fitting in the sense of still reproducing low values for E_v^m, because both magnitudes, being controlled by different potential details, appear only loosely coupled.

Present calculations predict the stability of 2D small vacancy clusters against 3D ones at the expense of a significant contribution of the entropy term to the free energy; the same relative stability was obtained previously using pseudopotential theory but based only on the configurational energy [33].

Regarding the self-interstitials, a review of results obtained with present day's most reliable EAM potentials indicates that a configuration along the compact row, either basal crowdion or basal dumbell, is the stable one. Such a defect migrates essentially in 1D, the possibility of 2D migration being much reduced. Both results are hardly consistent with available experimental data [24,34]. We believe that new HDS and internal friction experiments in single crystals, the first particularly searching for $\pi^{(2)}$ invariant, and the second to confirm the frozen-free split and identify proper compliances, can shed some light on the matter.

Acknowledgements

The work was partially supported by the Agencia Nacional de Promoción Científica y Tecnológica, Proyecto PMT-PICT0362, Argentina. The authors would like to thank Dr E.J. Savino and Dr F. Povolo for fruitful discussions, and Dr H. Jónsson for having sent us a new version of his Zr interatomic potential.

References

[1] D.J. Oh, R.A. Johnson, J. Mater. Res. 3 (1988) 471.
[2] D.J. Oh, R.A. Johnson, J. Nucl. Mater. 169 (1989) 5.
[3] M. Igarashi, M. Khantha, V. Vitek, Philos. Mag. B 63 (1991) 603.
[4] M.S. Daw, M.I. Baskes, Phys. Rev. B 29 (1984) 6443.
[5] M.W. Finnis, J.E. Sinclair, Philos. Mag. A 50 (1984) 45.
[6] R. Pasianot, E.J. Savino, Phys. Rev. B 45 (1992) 12704.
[7] G.J. Ackland, Philos. Mag. A 66 (1992) 917.
[8] G.J. Ackland, S.J. Wooding, D.J. Bacon, Philos. Mag. A 71 (1995) 553.
[9] E.S. Fisher, C.J. Renken, Phys. Rev. 135 (1964) A482.
[10] A.S. Goldstein, H. Jónsson, Philos. Mag. B 71 (1995) 1041.
[11] R. Pasianot, D. Farkas, E.J. Savino, Phys. Rev. B 43 (1991) 6952.
[12] J.R. Smith, D.J. Srolovitz, Modelling Simul. Mater. Sci. Eng. 1 (1992) 101.
[13] D.J. Bacon, J. Nucl. Mater. 206 (1993) 249.
[14] M.I. Baskes, R.A. Johnson, Modelling Simul. Mater. Sci. Eng. 2 (1994) 147.
[15] W.B. Pearson, A Handbook of Lattice Spacings and Structures of Metals and Alloys, Pergamon, Oxford, 1967.
[16] C. Kittel, Introduction to Solid State Physics, Wiley, New York, 1986.
[17] G.M. Hood, J. Nucl. Mater. 139 (1986) 179.
[18] J.H. Rose, J.R. Smith, F. Guinea, J. Ferrante, Phys. Rev. B 29 (1984) 2963.
[19] M.J. Norgett, R.C. Perrin, E.J. Savino, J. Phys. F 2 (1972) L73.

[20] J.R. Fernández, A.M. Monti, Phys. Status Solidi B 179 (1993) 337.
[21] J.R. Fernández, A.M. Monti, R.C. Pasianot, J. Nucl. Mater. 229 (1995) 1.
[22] J.R. Beeler Jr., in: S. Amelinckx, R. Gevers, J. Nihoul (Eds.), Radiation Effects Computer Experiments, North-Holland, Amsterdam, 1983.
[23] P. Bisio, A.M. Momti, Phys. Status Solidi B 135 (1986) 545.
[24] P. Ehrhart, B. Schönfeld, in: V. Takamura, J. Doyama, M. Kiritani (Eds.), Proceedings of Yamada Conference on Point Defects and Defect Interactions in Metals, Tokyo University, 1982, p. 47.
[25] M. Fuse, J. Nucl. Mater. 136 (1986) 250.
[26] A.M. Monti, Phys. Status Solidi B 167 (1991) 37.
[27] G.M. Hood, R.J. Schultz, J.A. Jackman, J. Nucl. Mater. 126 (1984) 79.
[28] A.D. King, G.M. Hood, R.A. Holt, J. Nucl. Mater. 185 (1991) 174.
[29] G.M. Hood, Defect Diffus. Forum 95–98 (1993) 755.
[30] G.M. Hood, R.J. Schultz, N. Matsuura, J. Nucl. Mater. 226 (1995) 260.
[31] G.M. Hood, H. Zou, R.J. Schultz, N. Matsuura, J.A. Roy, J.A. Jackman, Defect Diffus. Forum 143–147 (1997) 49.
[32] J. Horváth, F. Dyment, H. Meherer, J. Nucl. Mater. 126 (1984) 206.
[33] V.G. Kapinos, Yu.N. Osetsky, P.A. Platonov, J. Nucl. Mater. 195 (1992) 83.
[34] R. Pichon, E. Bisogni, P. Moser, Radiat Eff. 20 (1973) 159.
[35] A.S. Nowick, B.S. Berry, Anelastic Relaxation in Crystalline Solids, Academic Press, New York, 1972.
[36] P. Ehrhart, B. Schönfeld, Phys. Rev. B 19 (1979) 3896.